Fabrication and Local Electrical Characterization of p-n Junction Copper Phthalocyanine Nanorods

Koshiba, Yasuko
Sugimoto, Iori
Horike, Shouhei
Fukushima, Tatsuya
Ishida, Kenji

(Citation)
physica status solidi (a),220(24):2300243

(Issue Date)
2023-07-29

(Resource Type)
journal article

(Version)
Accepted Manuscript

Fabrication and Local Electrical Characterization of p–n Junction Copper Phthalocyanine Nanorods

Yasuko Koshiba, Iori Sugimoto, Shohei Horike, Tatsuya Fukushima, Kenji Ishida**

Y. Koshiba[1,2], I. Sugimoto[1], S. Horike[1,2], T. Fukushima[1,2], K. Ishida[1,2,3]

1. Department of Chemical Science and Engineering, Graduate School of Engineering, Kobe University, 1-1 Rokkodai-cho Kobe 657-8501, Japan

2. Research Center for Membrane and Film Technology, Kobe University, 1-1 Rokkodai-cho Kobe 657-8501, Japan

3. Department of Quantum Physics and Nuclear Engineering, Graduate School of Engineering, Kyushu University, 744 Motooka Nishi-ku Fukuoka 819-0395, Japan

E-mail: koshiba@kobe-u.ac.jp, ishida.kenji.383@m.kyushu-u.ac.jp

Keywords: organic semiconductor, p–n junction, nanorod, phthalocyanine, conductive AFM

One-dimensional (1D) organic semiconductor nanostructures have attracted considerable attention; however, only a few studies have been conducted on p–n junction organic semiconductor 1D nanostructures. In this study, p- and n-type and p–n junction phthalocyanine (Pc) nanorods are grown in the out-of-plane direction of a substrate via vacuum deposition using typical organic semiconductors with copper phthalocyanine (CuPc) as the p-type semiconductor and copper octafluorophthalocyanine (F_8CuPc) and copper hexadecafluorophthalocyanine (F_{16}CuPc) as the n-type semiconductors. P–n junction Pc nanorods are fabricated via the continuous deposition of F_8CuPc and F_{16}CuPc onto CuPc nanorods. Fourier-transform infrared spectroscopy reveals that the Pc molecules in the nanorods are perpendicularly aligned, with their molecular planes oriented toward the longitudinal direction of the nanorods. The local current–voltage properties of the nanorods are measured using conductive atomic force microscopy. The hole mobility in the CuPc nanorods is 10-times higher than that in the CuPc thin films. The p–n junction properties of F_8CuPc/CuPc nanorods are evaluated.

1. Introduction

One-dimensional (1D) organic semiconductor nanostructures, such as nanorods, nanowires, and nanopillars, are expected to exhibit anisotropic optical and electrical properties.[1–4] Metal phthalocyanines (MPcs) are promising organic semiconductors with desirable properties including non-toxicity, high chemical and thermal stabilities, and excellent optical properties. They are used as active layers in various devices, such as organic solar cells,[5–8] organic transistors,[9–11] and gas sensors.[12–14] Pcs have extended π-conjugation on their molecular planes and aggregate in the direction of stacking molecular planes, which are favorable for charge transport, owing to their π–π interactions.[15–17] Therefore, the 1D nanostructures of Pcs are promising building blocks for high-performance and high-integration nanodevices. Various methods have been reported for controlling the 1D nanostructures of Pc molecules, including physical vapor deposition,[18–21] solution processes,[22–24] vacuum deposition on Au,[25–27] and using organic or inorganic semiconductors[7,28,29] and graphene substrates.[30] Numerous studies have been conducted on organic semiconductor p–n junctions. Several studies have demonstrated single-crystalline organic p–n heterojunctions fabricated using a solution-based process.[31–33] However, despite the increasing research interest in p–n junction organic semiconductor 1D nanostructures,[34–36] relevant studies are limited, owing to the difficult fabrication process. MPc molecules are p- or n-type molecules depending on their terminal substituents, and p–n junction Pc nanorod arrays could be building blocks for a sensitive photo sensor. To fabricate nanorod arrays, nanorod growth in the out-of-plane direction of the substrate is suitable. The orientation of MPc molecules in MPc thin films prepared via vacuum deposition is dependent on the surface energy of the substrate;[37] therefore, selecting an appropriate substrate species is important for controlling the direction of rod growth. In our previous studies, we fabricated p- and n-type Pc nanorods using chemical vapor and vacuum depositions.[38–40]

In this study, we focused on the fabrication of MPc p–n junction nanorod arrays grown in the out-of-plane direction of the substrate, which has rarely been reported. We attempted to fabricate p–n junction nanorods via continuous vacuum deposition using Copper phthalocyanine (CuPc) as the p-type organic semiconductor and copper octafluorophthalocyanine (F_8CuPc) and copper hexadecafluorophthalocyanine (F_{16}CuPc) as the n-type organic semiconductors; therefore, both the p- and n-type molecules possessed the same Pc backbone. Further, for nanorod growth, a Au thin film was used as a substrate, on which the CuPc molecules were adsorbed in a face-on orientation.

Furthermore, the electrical characterization of nanorod arrays grown in the out-of-plane direction is difficult using typical sandwich devices, owing to leakage caused by the metal deposited for the top electrode entering the gaps between the nanorods. Therefore, we focused on the conductive atomic force microscopy (c-AFM) method,[41–43] which can effectively be employed for local electrical characterization via sweeping the voltage using a conductive cantilever as the upper electrode. c-AFM can be used for the electrical characterization of a small region of nanorods grown in the out-of-plane direction.

In this study, we investigated the fabrication of p- and n-type and p–n junction MPc nanorods grown in the out-of-plane direction of a substrate by appropriately selecting the substrate species and controlling the substrate temperature using vacuum deposition. To fundamentally evaluate the MPc nanorods, the orientation of its molecules and local electrical properties were evaluated.

2. Results and Discussion

2.1. Fabrication of p- and n-type MPc Nanorods

Before fabricating the p–n junction nanorods, the conditions for p- and n-type Pc nanorod formations were investigated by controlling the substrate temperature using Cr/Au-deposited Si substrates. The chemical structures of CuPc, F_8CuPc, and F_{16}CuPc are shown in **Figure 1.**

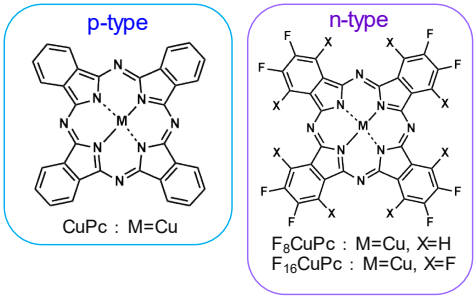

Figure 1. Chemical structures of CuPc, F_8CuPc, and F_{16}CuPc

Figure 2 shows the surface and cross-sectional scanning electron microscopy (SEM) images of the p-type CuPc thin films on the Si and Si/Cr/Au substrates fabricated at a substrate temperature (T_s) of room temperature (RT) and 110 °C. The film thickness was maintained at 80 nm to monitor the quartz crystal microbalance during vacuum deposition. At RT, the vacuum-deposited CuPc film on the Si substrate comprised small particles with diameters of 20–40 nm (Figure 2(a)). Particles with diameters of 10–30 nm were also observed on the Si/Cr/Au substrate (Figure 2(b)). Notably, the thin-film morphology changes at 110 °C, as shown in the surface image of the CuPc thin film deposited on the Si substrate in Figure 2(c). Long-growing shapes with widths of approximately 50 nm were observed in the in-plane direction of the substrate. The cross-sectional image of this thin film in Figure 2(c) (lower part) shows that the film thickness is uniform and approximately 80 nm. These results suggest that the in-plane rod growth on the Si substrate occurred at 110 °C, whereas the out-of-plane growth of the CuPc nanorods (diameter of approximately 45 nm) on the Si/Cr/Au substrate was observed at 110 °C.

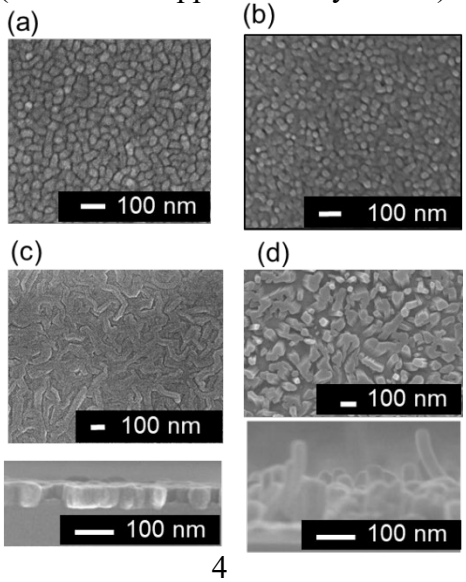

Figure 2. Surface SEM images of the CuPc thin films vacuum-deposited on (a) Si and (b) Si/Cr/Au substrate at RT. Surface (top) and cross-sectional (bottom) SEM images of the CuPc thin film vacuum-deposited on (c) Si and (d) Si/Cr/Au substrates at 110 °C

The n-type F_8CuPc and F_{16}CuPc thin films were prepared using vacuum deposition under the same conditions as those for the preparation of the p-type CuPc thin films. The morphologies of the films were analyzed using SEM. **Figure 3** shows the surface and cross-sectional SEM images of the F_8CuPc and F_{16}CuPc thin films deposited on the Si/Cr/Au substrates at 110 °C. The film thicknesses were 50 and 80 nm for F_8CuPc and F_{16}CuPc, respectively. Notably, out-of-plane nanorod growth was observed in both the F_8CuPc and F_{16}CuPc thin films. The rod diameters were approximately 41 and 32 nm for F_8CuPc and F_{16}CuPc, respectively. The rod diameter of F_8CuPc was slightly smaller than that of CuPc (approximately 45 nm). In F_{16}CuPc, in which all the H atoms at the end of the Pc ring were replaced by F atoms, the diameter was >10 nm smaller than that in CuPc.

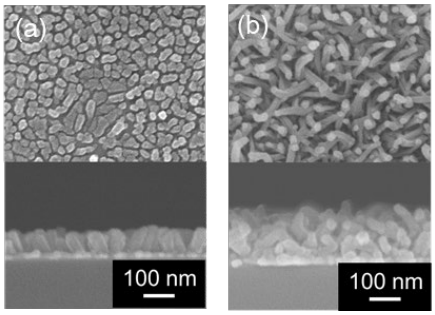

Figure 3. Surface (top) and cross-sectional (bottom) SEM images of (a) F_8CuPc and (b) F_{16}CuPc thin films vacuum-deposited at 110 °C on a Si/Cr/Au substrate

The molecular orientations of CuPc, F_8CuPc, and F_{16}CuPc in the nanorods were examined using transmission infrared (IR) spectroscopy and IR reflection absorption spectroscopy (RAS) measurements. In transmission measurements, molecular vibrations with transition moments in the in-plane direction of the substrate are strongly detected. Conversely, in RAS measurements, molecular vibrations with transition moments perpendicular to the substrate can be strongly detected, whereas molecular vibrations parallel to the substrate are difficult to

detect. Therefore, the molecular orientation can be evaluated using transmission and RAS measurements. The transmission IR spectrum of CuPc in a KBr pellet and the RAS profiles of CuPc, F_8CuPc, and F_{16}CuPc nanorod thin films are shown in **Figure 4**.

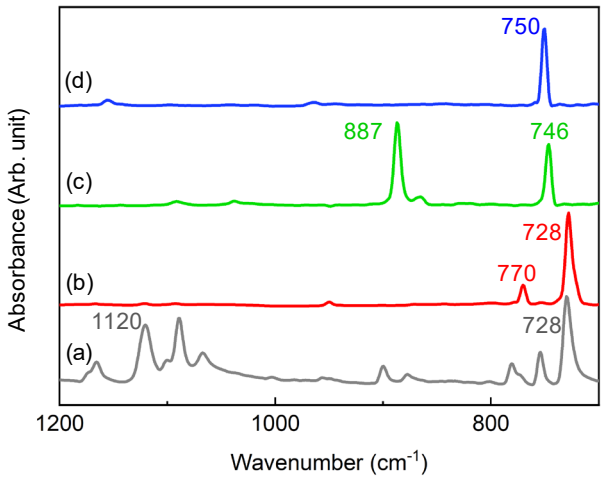

Figure 4. (a) Fourier transform infrared (FT-IR) spectrum of CuPc powder in KBr pellets. RAS profiles of (b) CuPc, (c) F_8CuPc, and (d) F_{16}CuPc nanorods

The spectrum of the CuPc powder (Figure 4(a)) showed absorption peaks corresponding to the Pc backbone between 700 and 1200 cm^{-1}. The absorption bands at 728 and 1120 cm^{-1} correspond to the out-of-plane (perpendicular to the molecular plane) and in-plane (parallel to the molecular plane) C–H bending modes of the benzene ring, respectively.[44–46] Both absorption peaks were distinctly observed in the spectrum of the CuPc powder. By contrast, a distinct peak corresponding to the out-of-plane C–H bending mode was observed at 728 cm^{-1} in the RAS profile of the CuPc nanorod thin film (Figure 4(b)); however, the in-plane C–H bending mode at 1120 cm^{-1} was not clearly observed. These results indicate that the CuPc molecules were aligned with a face-on orientation in the CuPc nanorods, and their molecular planes were oriented perpendicularly to the longitudinal direction of the nanorods. The transmission IR spectra of CuPc thin films vacuum-deposited onto the Si substrates at RT and 110 °C are shown in **Figure S1**. In the IR spectra of the thin films prepared at both T_s values of RT and 110 °C, strong peaks for the out-of-plane C–H bending mode were observed at 721

cm^{-1}, and small absorption peaks were observed at 1120 cm^{-1}. These results suggest that the CuPc molecules on the Si substrate were obliquely aligned with an edge-on orientation.

The orientation of CuPc molecules in vacuum-deposited films varies depending on the surface energy of the substrate and interaction between the substrates and molecules.[16,24–27, 31] Typically, on Si or glass substrates, CuPc molecules are aligned with an edge-on orientation, whereas on Au substrates, CuPc molecules are aligned with face-on orientation. Pc molecules aggregate owing to their π–π interactions.[15–17] Increasing the substrate temperature during vacuum deposition may increase the mobility of the molecules that are adsorbed onto the substrate. Furthermore, the π–π interactions act as a driving force in this system, thereby resulting in the aggregation of CuPc molecules and the formation of 1D nanorods. Consequently, on the Si substrate, the edge-on-oriented CuPc molecules aggregated in the π–π stacking direction, and CuPc rods grew in the in-plane direction (Figure 2(c)). By contrast, on the Au substrate, the face-on-oriented CuPc molecules stacked in the out-of-plane direction, and nanorods grew in the out-of-plane direction (Figure 2(d)). **Figure S2** shows the RAS spectra of the CuPc nanorods and thin films deposited on the Si/Cr/Au substrates at T_s = 110 °C and RT, respectively. The peak of the in-plane C–H bending mode at 1120 cm^{-1} was not clearly observed in the RAS spectrum of the CuPc nanorod thin film (Figure S2(a)). However, a weak peak was present at 1121 cm^{-1} in the RAS spectrum of the CuPc thin film (Figure S2(b)). These results indicate that the face-on orientation was dominant in CuPc thin films deposited at RT; however, an edge-on oriented component was also present. Therefore, the orientation of CuPc molecules was enhanced by the formation of nanorods.

Out-of-plane X-ray diffraction (XRD) patterns of CuPc nanorods and thin films deposited on the Si/Cr/Au substrates at T_s = 110 °C and RT, respectively, are shown in **Figure S3**. These results revealed that the CuPc thin films and nanorods were α-phase crystalline structures. The two XRD peaks in the pattern of the CuPc thin film (Figure S3(b)) revealed lattice spacings of 0.325 and 0.130 nm, which were attributed to the face- and edge-on orientations of the CuPc

molecules, respectively. In the XRD pattern of the CuPc nanorod thin film (Figure S3(a)), only one peak at 0.325 nm was observed, thereby suggesting that the molecular orientation was improved by nanorod formation. Owing to the change in molecular orientation, comparing the crystallinity between the thin films and nanorods is challenging. Therefore, the crystallite size was calculated from the peak at 0.325 nm using the Scherrer equation. The calculated crystallite sizes of the CuPc thin film and nanorods were 23.8 and 33.7 nm, respectively. Therefore, the crystallite size increased with nanorod formation.

The RAS profile of the F_8CuPc nanorod thin film (Figure 4(c)) showed a strong out-of-plane C–N–C deformation absorption peak at 746 cm^{-1} and an out-of-plane C–H motion peak at 887 cm^{-1}.[47] However, the in-plane C–H bending mode absorption peak at approximately 1110 cm^{-1} was not observed. The RAS profile of the F_{16}CuPc nanorod thin film (Figure 4(d)) showed a strong absorption peak assigned to the out-of-plane C–N–C deformation.[48] Regarding F_{16}CuPc, all atoms bonded to the benzene ring are F; therefore, out-of-plane C–H motion peak was not observed. Additionally, the out-of-plane C–F motion peak is generally observed in the wavenumber region of <600 cm^{-1},[47, 48] which is below the detection limit of the MCT detector. Therefore, this peak could not be observed in this experiment using the MCT detector. The F_8CuPc and F_{16}CuPc molecules in the nanorod thin films were also aligned with a face-on orientation. Similar to that for the CuPc rod formation, Pc molecules were adsorbed onto the Au substrates with a face-on orientation and aggregated owing to their π–π interactions. These results suggest that the π–π stacking direction favorable for charge transport was the longitudinal direction of both p- and n-type Pc nanorods.

2.2. Fabrication of p–n Junction MPc Nanorods

To fabricate p–n junction nanorods, CuPc (p-type) was vacuum-deposited on the Si/Cr/Au substrates at 110 °C, and F_8CuPc and F_{16}CuPc (n-type) were deposited continuously under vacuum. **Figure 5**(a) shows the cross-sectional SEM image of an 80 nm-thick F_{16}CuPc thin

film deposited on an 80 nm-thick CuPc layer. Nanorods with a length of 100–400 nm were observed in the CuPc/F_{16}CuPc stacked thin films. The CuPc/F_{16}CuPc nanorods grew longer than the CuPc nanorods, and the diameters of certain nanorods in the middle section changed. A magnified SEM image of the CuPc/F_{16}CuPc nanorods is shown in Figure 5(b). The diameters of the CuPc/F_{16}CuPc nanorods changed from 48 nm at the bottom part to 33 nm at the bottom and top parts. These values were comparable to the diameters of the CuPc and F_{16}CuPc nanorods. Figure 5(c) shows the cross-sectional SEM image of a 50 nm-thick F_8CuPc thin film deposited on a 50 nm-thick CuPc layer. Nanorods with lengths between 50 and 250 nm were observed in the CuPc/F_8CuPc stacked thin films. The CuPc/F_8CuPc nanorods were longer than the CuPc and F_8CuPc nanorods. However, no significant change was observed in the diameter of the nanorods because the diameter of F_8CuPc rods is approximately 41 nm, which is similar to that of the CuPc rods (approximately 45 nm).

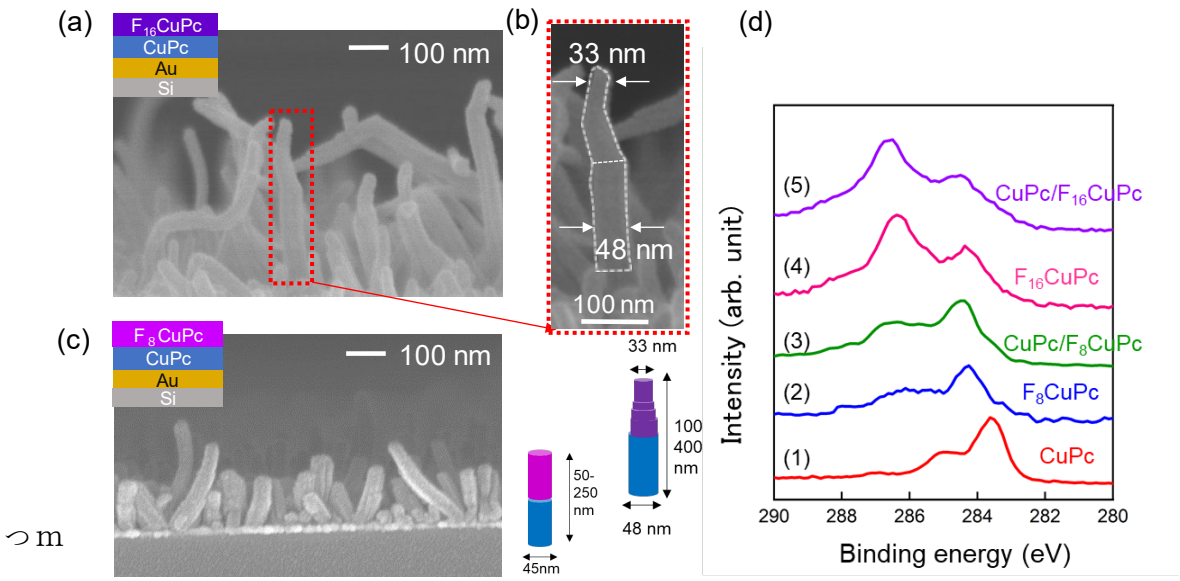

Figure 5. Cross-sectional SEM image of (a) CuPc/F_{16}CuPc thin film continuously vacuum-deposited on a Si/Cr/Au substrate at 110 °C. (b) Magnified image of the nanorods. (c) Cross-sectional SEM image of the CuPc/F_8CuPc thin film continuously vacuum-deposited on a Si/Cr/Au substrate at 110 °C. (d) X-ray photoelectron spectroscopy (XPS) C 1s spectra of (1) CuPc, (2) F_8CuPc, (3) CuPc/F_8CuPc, (4) F_{16}CuPc, and (5) CuPc/F_{16}CuPc nanorod thin films

XPS of the nanorod thin films was performed to confirm the formation of p–n junction nanorods. The C 1s high-resolution XPS profiles of the p- and n-type and p–n junction nanorod thin films are shown in Figure 5(d). In the C 1s spectrum of the CuPc nanorod film (Figure 5(d)(1)), the peaks observed at 283.5 and 284.8 eV correspond to the C–H bond of the benzene ring and Pc framework, respectively. In the C 1s spectrum of the F_{16}CuPc nanorod thin film (Figure 5(d)(4)), the peaks observed at 284.3 and 286.4 eV correspond to the Pc backbone and C–F bond, respectively.[49–51] In the C1s spectrum of the CuPc/F_{16}CuPc stacked nanorod thin film (Figure 5(d)(5)), the peaks observed at 284.3 and 286 eV correspond to the Pc backbone and C–F bond, respectively. Therefore, the C 1s spectrum of the CuPc/F_{16}CuPc stacked nanorod thin film was similar to that of the F_{16}CuPc nanorod thin film, thereby confirming the presence of F_{16}CuPc on the upper surface of the CuPc/F_{16}CuPc nanorod thin films. In the C 1s spectra of the F_8CuPc and CuPc/F_8CuPc nanorod thin films (Figure 5(d)(2) and 5(d)(3), respectively), similar peaks were observed at 284.4 eV. This result indicates the presence of F_8CuPc on the upper surface of the CuPc/F_8CuPc nanorods. XPS measurements revealed the presence of n-type Pc molecules on the top surface of the p–n stacked nanorod thin films. Morphological observations obtained using SEM and XPS measurements suggested the growth of the p–n junction of Pc nanorods in the out-of-plane direction on the Si/Cr/Au substrates via the continuous deposition of p- and n-type Pc molecules under vacuum at T_s = 110 °C.

2.3. Local Electrical Characterization using c-AFM

To evaluate the local electrical properties of nanorods, current–voltage *(I–V)* measurements were performed using c-AFM. A schematic of the measurement system is shown in **Figure 6**(a). The bottom electrode was a Cr/Au deposition film, and the top electrode was a conductive Pt-coated cantilever. The current image was measured simultaneously with the

topography in the contact mode, and the *I–V* curve was measured under vacuum (1×10^{-2} Pa) at an arbitrary location after the surface topography was observed.

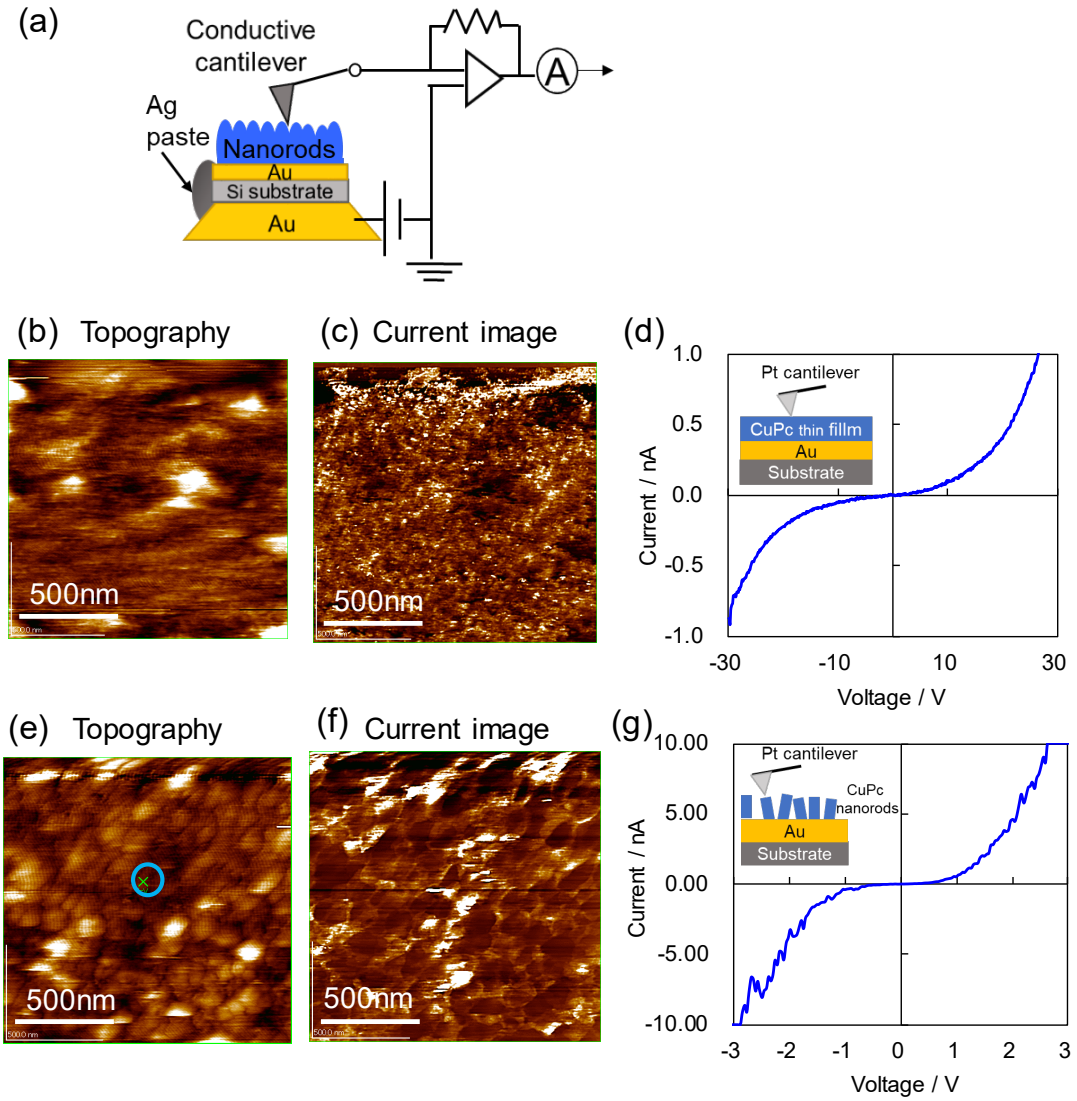

Figure 6. (a) Experimental setup for c-AFM measurements. (b) Topography, (c) current image, and (d) I–V curve of CuPc thin film deposited on the Si/Cr/Au substrate at RT. (e) Topography, (f) current image, and (g) *I–V* curve of CuPc nanorod thin films on the Si/Cr/Au substrate at 110 ºC. All measurements are performed using the c-AFM method

First, the p-type CuPc thin films and nanorods were evaluated. Figure 6(b) and (c) show the topography and current images, respectively, of the CuPc thin film deposited on the Si/Cr/Au substrate at 50 nm at T_s = RT measured at an applied voltage of 3 V. The topography showed CuPc grains with a maximum height difference (*Rz*) of 29.1 nm and mean square roughness (*Rq*) of 2.75 nm. In the current image, the current value was low in the thick part of the film

and high in the thin part, which was consistent with the topography results. The *I–V* curve of the CuPc thin film is shown in Figure 6(d). Using the log plot of the *I–V* curve, ohmic and space-charge-limited current (SCLC) regions were identified at both positive and negative voltages. The hole mobility (μ) of the SCLC region in the CuPc thin film was $1.43 \pm 0.32 \times 10^{-4}$ cm^2/Vs. This value is comparable to that of the CuPc film obtained from the *I–V* curve measured using the vertical device with a deposited Au top electrode.

Figure 6(e) and (f) show the topography and current images of 30 nm-thick CuPc nanorod thin films deposited on a Si/Cr/Au substrate at 110 ℃ measured at an applied voltage of 3 V, respectively. The topography showed CuPc nanorods with *Rz* and *Rq* values of 29.1 and 2.75 nm, respectively. As evident from the cross-sectional SEM image of this film, the length of the CuPc nanorods was approximately 30–50 nm, and the *Rz* value was approximately 40.5 nm, which were similar to those of the nanorods. Further, rod shapes were observed. In the current image, the current value was low in the thick part of the film and high in the thin part, which was consistent with the topography results. The *I–V* curve was measured at the indicated area in Figure 6(e). Ohmic and SCLC regions were identified at both positive and negative voltages. The μ value of the CuPc nanorod thin film in the SCLC region was $3.44 \pm 2.05 \times 10^{-3}$ cm^2/Vs, which was 10-times higher than that in the CuPc thin films. The RAS spectra of the CuPc nanorods show that the formation of CuPc nanorods enhanced the molecular orientation, and the XRD measurements show that the crystal crystallite size increased with nanorod formation. Therefore, the formation of CuPc nanorods resulted in improved carrier mobility.

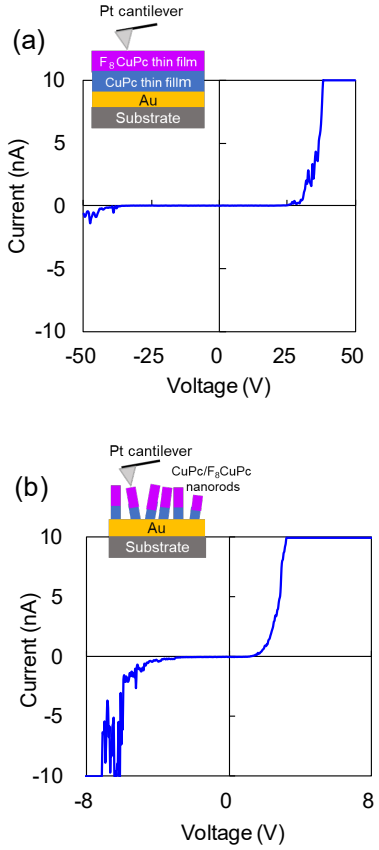

Figure 7. *I–V* curves of (a) CuPc/F_8CuPc stacked thin film deposited on the Si/Cr/Au substrate at RT and (b) CuPc/F_8CuPc CuPc nanorod thin film on the Si/Cr/Au substrate at 110 °C, measured using the c-AFM method.

Next, the p–n stacked thin films of F_8CuPc on the CuPc and CuPc/F_8CuPc p–n junction nanorod thin films were similarly evaluated using the Pt cantilever system. **Figure 7**(a) shows the *I–V* curve of the CuPc/F_8CuPc stacked thin film deposited at T_s = RT. The thicknesses of CuPc and F_8CuPc films were 500 and 200 nm, respectively. The shape of the *I–V* curve is similar for positive and negative voltages for the CuPc thin film (Figure 6(d)). However, the shape of the *I–V* curve differed between the positive and negative voltages for the CuPc/F_8CuPc stacked thin film, and the current flow was difficult to achieve at the negative voltages. These *I–V* characteristics differ from those of the p-type CuPc thin film. This difference in *I–V* characteristics may be due to the formation of a depletion layer between the CuPc and F_8CuPc layers upon the application of a negative voltage.

Figure 7(b) shows the *I–V* curve of the CuPc/F_8CuPc nanorod thin film deposited at T_s = 110 °C. This p–n junction nanorod thin film was fabricated using continuous vacuum deposition as follows. In brief, a 30 nm-thich film of CuPc was vacuum-deposited onto a Si/Cr/Au substrate at 110 °C. Subsequently, a 30 nm-thick film of F_8CuPc was continuously vacuum-deposited onto the CuPc nanorods. For the CuPc/F_8CuPc nanorod thin film, at a positive voltage, the current value increased from approximately 1.6 V, whereas at a negative voltage, the current value increased from approximately –3.2 V. Similar to that for the CuPc/F_8CuPc p–n stacked thin film, achieving current flow at a negative voltage was difficult, owing to the formation of a depletion layer. These results indicate that the local electrical properties of the CuPc/F_8CuPc p–n junction nanorods may be measured using c-AFM.

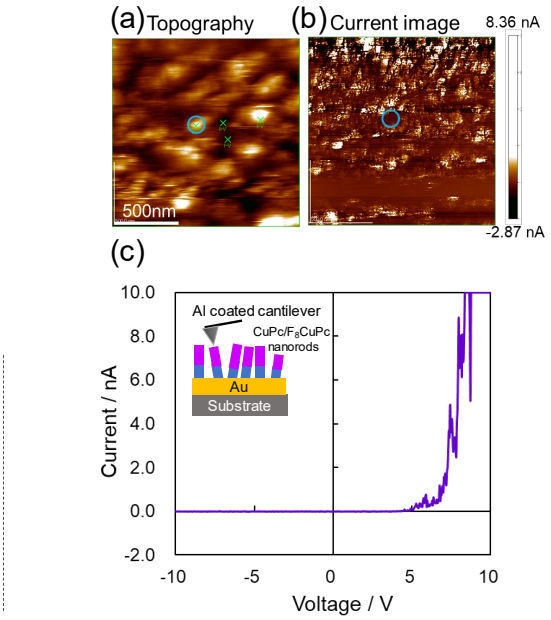

Figure 8. (a) Topography, (b) current image, and (c) *I–V* curve of the CuPc/F_8CuPc p–n junction nanorods measured using the c-AFM method.

Finally, the local *I–V* measurements of the p–n junction CuPc/F_8CuPc nanorods were obtained via vacuum-depositing an 80 nm-thick layer of Al onto the conductive Pt-coated cantilever. In these measurements, the bottom and top electrodes were Cr/Au and Al, respectively. The topography and current images of the p–n junction CuPc/F_8CuPc nanorod thin film are shown in **Figure 8**(a) and (b), respectively. Rod-like structures were observed in the topography

image, and a current image corresponding to the topography results was obtained. The local *I–V* measurement was performed at the center of the circle indicated in Figure 8(a). As shown in Figure 8(c), no current is observed during the negative voltage sweep, whereas the current increases with increasing voltage during the positive voltage sweep, thereby indicating a significant rectification property of this system. Local electrical measurement using c-AFM enabled the characterization of the p–n junction properties of the MPc p–n junction nanorods.

3. Conclusions

In this study, we focused on the 1D p–n junctions of organic semiconductors and attempted to fabricate p–n junction nanorods with Pc compounds using vacuum deposition by controlling *Ts*. Herein, p- and n-type and p–n junction MPc nanorods were fabricated using CuPc as the p-type semiconductor and F_{16}CuPc and F_8CuPc as the n-type semiconductors. In both p- and n-type Pc nanorods, Pc molecules exhibited a face-on orientation. Moreover, the π–π stacking direction, which is favorable for charge transport, was the longitudinal direction of the nanorods. Further, p–n junction nanorods were fabricated via the continuous vacuum deposition of n-type F_8CuPc and F_{16}CuPc on p-type CuPc nanorods. SEM observations and XPS measurements confirmed the formation of p–n junction Pc nanorods.

Electrical characterization of the nanorods, with diameters of approximately 40 nm, was performed via local electrical measurements using c-AFM. Current images corresponding to the topography images were obtained using a conductive cantilever. The local *I–V* measurements on the CuPc nanorod revealed that the carrier mobility of the CuPc nanorods was $3.44 \pm 2.05 \times 10^{-3}$ cm^2/Vs, which was 10-times higher than that of the CuPc thin film. The *I–V* curves of the CuPc/F_8CuPc nanorods measured with the Al-deposited conductive cantilever as the top electrode showed clear rectification, thereby enabling us to determine the characteristics of the p–n junction nanorods. This study is a fundamental evaluation of

fabricated organic semiconducting p–n junction nanorods. We demonstrated that the c-AFM method is effective for the electrical characterization of nanorod thin films, which is difficult to achieve because of leakage in devices with the vertical structures that use deposited metal films as a top electrode. We successfully achieved the fundamental electrical characterization of p-type and p–n junction Pc nanorods. Although further experiments are required, the fabricated p–n junction Pc nanorods show potential for diverse practical applications, such as optical sensors.

4. Experimental Section/Methods

CuPc (Tokyo Chemical Industries, Japan) was purified via sublimation and used as the p-type Pc, whereas F_8CuPc (Tokyo Chemical Industries, Japan) and F_{16}CuPc (Tokyo Chemical Industries, Japan) were purified by sublimation and used as the n-type Pc. Cr (5 nm) and Au (35 nm) were vacuum deposited onto a Si substrate. CuPc, F_8CuPc, and F_{16}CuPc were deposited onto a Si or Si/Cr/Au substrate at RT or 110 °C at a deposition rate of 0.02–0.05 nm/s and 5×10^{-4} Pa. The morphologies of the Pc nanorods and thin films were investigated using field-emission SEM (JEOL JSM-7500F, Japan). The Pc nanorods were examined using FT-IR spectroscopy (JASCO FT/IR-600 Plus, Japan) in the RAS mode and XPS (ULVAC-PHI PHI X-tool, Japan). XRD patterns were measured using a Rigaku Ultima IV instrument (Japan). The local electrical characteristics of the Pc nanorods and thin films were measured using c-AFM (SII SPI3800N, Japan).

Acknowledgements

This work was partially supported by JSPS KAKENHI and the Kawanishi Memorial ShinMaywa Education Foundation.

Received: ((will be filled in by the editorial staff))
Revised: ((will be filled in by the editorial staff))
Published online: ((will be filled in by the editorial staff))

References

[1] Y-L. Shi, X-D. Wang, *Adv. Funct. Mater.* **2021**, *31*, 2008149.

[2] H. Zhu, Y. Fu, F. Meng, X. Wu, Z. Gong, Q. Ding, M. V. Gustafsson, M. T. Trinh, S. Jin, X-Y. Zhu, *Nat. Mater.* **2015**, *14*, 636.

[3] Y. S. Zhao, H. Fu, A. Peng, Y. Ma, Q. Liao, J. YAO, *Acc. Chem. Res.* **2010**, *43*, 3, 409.

[4] D. K. Jones, M. Kertesz, N. Gavvalapalli, *Cryst. Growth Des.* **2021**, *21*, 2465.

[5] P. Peumans, R. Forrest, *Appl. Phys. Lett*. **2001**, *29*, 126.

[6] B. H. Lessar, *ACS Appl. Mater. Interfaces* **2021**, *13*, 31321.

[7] M. Shahiduzzaman, T. Horikawa, T. Hirayama, M. Nakano, M. Karakawa, K.Takahashi, J-M. Nunzi, T. Taima, *J. Phys. Chem. C* **2020**, *124*, 21338.

[8] K. Suemori, T. Miyata, M. Yokoyama, M. Hiramoto, *Appl. Phys. Lett*. **2005**, *86*, 063509.

[9] T. Yasuda, T. Tsutsui, *Chem. Phys. Lett.* **2005**, *402*, 395.

[10] B. Q. Tang, H. Li, M. He, W. Hu, C. Liu, K. Chen, C. Wang, Y. Liu, D. Zhu, *Adv. Mater.* **2006**, *18*, 65–68

[11] J. Mei, Y. Diao, A. L. Appleton, L. Fang, Z. Bao, *J. Am. Chem. Soc*. **2013**, *135*, 6724−6746

[12] M. Bouve, *Anal. Bioanal. Chem.* **2006**, *384*, 366.

[13] S. Kumar, A. K. Sharma, M. K. Sohal, D. P. Sharama, A. K. Debnath, D. K. Aswal, A. Mahajun, *Sens. Actuators B Chem.* **2021**, *327*, 128925.

[14] I. Muzikante, V. Parra, R. Dobulans, E. Fonavs, J. Latvels, M. Bouvet, *Sensors* **2007**, *7*, 2984.

[15] G. de la Torre, C. G. Claessens, T. Torres, *Chem. Commun*. **2007**, 2000.

[16] Y. Wu, X. Zhang, H. Pan, X. Zhang, Y. Zhang, X. Zhang, J. Jie, *Nanotechnology* **2013**, *24*, 35520.

[17] S-C. Suen, W-T. Wjang, F-J. Hou, B-T. Dai, *Org. Electron.* **2006**, *7*, 428.

[18] Y. Yoon, S. Kim, H. C. Choi, *NPG Asia Mater.* **2020**, *12*, 16.

[19] Y. Zhang, X. Wang, Y. Wu, J. Jie, X. Zhang, Y. Xing, H. Wu, B. Zou, *J. Mater. Chem.* **2012**, *22,* 14357.

[20] X. Wang, W. Wu, H. Ju, T. Zo, Z. Qiao, H. Gong, H. Wang, *Mater. Res. Express* **2016**, *3*, 125002.

[21] S. Y. Flores, J. Gonzalez-Espiet, J. Cintrón, N. D. J. Villanueva, F. E. Camino, K. Kisslinger, D. M. P. Cruz, R. D. Rivera, L. F. Fonseca, *ACS Appl. Nano Mater.* **2022**, *5*, 4688.

[22] T. Higashi, M. Ohmori, M. F. Ramananarivo, A. Fujii, M. Ozaki, *APL Mater*. **2015**, *3*, 126107.

[23] M. Samanta, P. Howli, U. K. Ghorai, M. Mukherjee, C. Bose, K. K. Chattopadhyay, *Physica E Low Dimens. Syst. Nanostruct.* **2019**, *114,* 113654.

[24] Y. Wu, J. Feng, X. Jiang, Z. Zhang, X. Wang, B. Su, L. Jiang, *Nat. Commun*. **2015**, *6*, 6737.

[25] B. N. Mbenkum, E. Barrena, X. Na. Zhang, M. Kelsch, H. Dosch, *Nano Lett.* **2006**, *6*, 2852.

[26] T. N. Krauss, E. Barrena, T. Lohmüller, M. Kelsch, A. Breitling, P. A. van Aken, J. P. Spatz, H. Dosch, *Chem. Mater.* **2009**, *21*, 5010.

[27] T. N. Krauss, E. Barrena, T. Lohmuller, J. P. Spatzac, H. Doschad, *Phys. Chem. Chem. Phys*. **2011**, *13*, 5940.

[28] M. Hirade, H. Nakanotani, M. Yahiro, C. Adachi, *ACS Appl. Mater. Interfaces* **2010**, *3*, 1*,* 80.

[29] Y. Zhou, T. Taima, T. Miyadera, T. Yamanari, M. Kitamura, K. Nakatsu, Y. Yoshida, *Nano Lett*. **2012**, *12*, 4146.

[30] D. L. G. Arellano, E. K. Burnett, S. D. Uzun, J. A. Zakashansky, V. K. Champagne, M. George, S. C. B. Mannsfeld, A. L. Briseno, *J. Am. Chem. Soc.* **2018**, *140*, 8185.

[31] C. Fan, A. P. Zoombelt, H. Jiang, W. Fu, J. Wu, W. Yuan, Y. Wang, H. Li, H. Chen, Z. Bao, *Adv. Mater.* **2013**, *25*, 5762.

[32] B. Peng, R. Wu, H. Li, *Acc. Chem. Res.* **2021**, *54*, 4498.

[33] M. Xiao, J. Liu, C. Liu, G. Han, Y. Shi, C. Li, X. Zhang, Y. Hu, Z. Liu, X. Gao, Z. Cai, J. Liu, Y. Yi, S. Wang, D. Wang, W. Hu, Y. Liu, H. Sirringhaus, L. Jiang, *Nat. Commun*. **2021**, *12*, 2774.

[34] Q. H. Cui , L. Jiang, C. Zhang, Y. S. Zhao, W. Hu, J. Yao, *Adv.Mater.* **2012**, *24*, 2332.

[35] Y. Zhang, H. Dong, Q. Tang, S. Ferdous, F. Liu, S. C. B. Mannsfeld, W. Hu, A. L. Briseno, *J. Am. Chem. Soc.* **2010**, *132*, 11580.

[36] J. Wu, Q. Li, G. Xue, H. Chen, H. Li, *Adv.Mater.* **2017**, *29*, 1606101.

[37] Y-S. Hsiao, W-T. Whang, S-C. Suen, J-Y Shiu, C-P Chen, *Nanotechnology*, **2008**, 19, 41, 415603.

[38] H. Saeki, M. Nishimoto, Y. Koshiba, M. Misaki, K. Ishida, Y. Ueda, *Thin Solid Films* **2013**, *531*, 513.

[39] Y. Koshiba, M. Nishimoto, A. Misawa, M. Misaki, K. Ishida, *Jpn. J. Appl. Phys.* **2016**, *55*, 03DD07.

[40] Y. Koshiba, T. Ohnishi, M. Morimoto, M. Misaki, T. Fukushima, K. Ishida, *Mol. Cryst. Liq. Cryst.* **2017**, *653*, 157.

[41] G. A. MacDonald, P. A. Veneman, D. Placencia, N. R. Armstrong, *ACS Nano* **2012**, *6*, *11*, 9623.

[42] J. M. Mativetsky, H. Wang, S. S. Lee, L. W. Brooksa, Y. L. Loo, *Chem. Commun.* **2014**, *50*, 5319.

[43] A. Stern, S. Aharon, T. Binyamin, A. Karmi, D. Rotem, L. Etgar, D. Porath, *Adv. Mater.* **2020**, *32*, 19078.

[44] S. Tokito, J. Sakata, T. Taga, *Thin Solid Films* **1995**, *256*, 182.

[45] M. K. Debe, K. K. Kan, *Thin Solid Films* **1990**, *186*, 289.

[46] A. A. M. Farag, *Opt. Laser Technol*. **2007**, *39*,728.

[47] D. D. Klyamera, A. S. Sukhikha, P. O. Krasnova, S. A. Gromilova, N. B. Morozovaa, T. V. Basovaa, *Appl. Surf. Sci.* **2016**, *372*, 79.

[48] T. V. Basovaa, N. S. Mikhaleva, A. K. Hassanc, V. G. Kiselevb, *Sens. Actuator B* **2016**, *227*, 634.

[49] D. G. de Oteyza, A. El-Sayed, J. M. Garcia-Lastra, E. Goiri, T. N. Krauss, A. Turak, E. Barrena, H. Dosch, J. Zegenhagen, A. Rubio, Y. Wakayama, J. E. Ortega, *J. Chem. Phys.* **2010**, *133*, 214703.

[50] H. Peisert, M. Knupfer, T. Schwieger, G. G. Fuentes, D. Olligs, J. Fink, T. Schmidt, *J. Appl. Phys.* **2003**, *93*, 968.

[51] H. Peisert, M. Knupfer, J. Fink, *Surf. Sci.* **2002**, *515*, 491.